Enhanced Monopole Antenna for On-Chip E-Band Applications

Karen N. Olan-Nuñez and Roberto S. Murphy-Arteaga

Abstract – We present the design of an enhanced monopole antenna for on-chip applications using a metasurface composed of an array of Jerusalem cross unit cells to improve the radiation and electrical properties. The monopole antenna operates from 67.83 GHz to 81.93 GHz, covering a part of the E-band. The achieved enhancement was from 1 to 2.33 dBi, from 0.02 dBi to 0.31 dBi, and from 19% to 49% for gain, directivity, and radiation efficiency, respectively, derived from full-wave simulations. The topology was designed on a 300 μm thickness high-resistivity silicon wafer and an 18 μm silicon dioxide insulation layer between the monopole antenna and metasurface. The total size of the proposed device is $1.2 \times 1.2 \times 0.330$ mm^3. The frequency range, size, simplicity, and materials used for the design are suitable for on-chip applications, such as in vehicular radar systems, as well as other E-band applications.

1. Introduction

To meet the huge public demand for compact, wireless systems, antennas, besides the other necessary electronic modules, must be integrated on the same silicon chip, and thus research on on-chip antennas has become a very important field of endeavor.

For years, in order to improve the gain, directivity, and radiation efficiency while keeping the size of the antennas small, different types of metamaterials have been proposed, such as artificial magnetic conductors [1, 2], high-impedance surfaces [3, 4], electromagnetic band rejecting structures [5], doubly negative materials [6, 7], zero-order resonators [8], composite left-right-handed metamaterials [9], and metasurfaces [10] and the use of split ring resonators and their complement [11–13].

In other works, external resonator substrates placed in the vicinity of the antenna [14] or lenses [15, 16] have been used. Other alternatives are 1) micromachining, which consists of the removal of small amounts of silicon under or in the vicinity of the radiating device [17]; 2) local doping around the antenna [18]; 3) optimization of the position so that the antenna has fewer devices nearby to avoid coupling, interference, and other parasitic effects [19]; 4) metallization of printed circuit board cards so that they act as reflectors [20]; and 5) the use of high-resistivity semiconductor substrates [21] to reduce losses due to the substrate.

This article is based on a conventional monopole antenna topology to design a new metamaterial-based antenna, keeping design simplicity and compactness while improving the gain, directivity, radiation efficiency, and impedance bandwidth. The enhanced monopole antenna was designed using a high-resistivity silicon (HR-Si) wafer, a silicon dioxide insulation layer, and copper metal layers.

Manuscript received 9 September 2022.

Karen N. Olan-Nuñez and Roberto S. Murphy-Arteaga are with the Electronics Department, Instituto Nacional de Astrofísica, Óptica y Electrónica (INAOE), Puebla, México, 72840; e-mail: Karen.olan@inaoep.mx; rmurphy@ieee.org.

2. Design

A conventional monopole antenna was previously designed to operate in a part of E-band range, from 76 GHz to 81 GHz, using a full-wave simulator. The monopole antenna without the metasurface is depicted in Figure 1, which also includes its dimensions.

The design of the well-known metamaterial unit cells (commonly named Jerusalem crosses) was carried out in the full-wave simulator, using the methodology shown in Figure 2 and proposed in [22], to extract the complex refractive index, complex permittivity, and complex permeability.

The metamaterial cells were designed iterating until an appreciable enhancement was attained for the monopole antenna. Roughly, the steps were as follows: 1) a metamaterial cell was modeled, 2) this primary metamaterial cell was arranged in an array above the monopole antenna, 3) the variation of position and distances was analyzed, and 4) the radiation and electric parameters were studied to judge if the achieved improvement was sufficient; otherwise, the iteration process was begun anew.

The right side of Figure 2 depicts the declaration of wave ports and perfect electrical conductor (PEC)–perfect magnetic conductor (PMC) boundary conditions used for the full-wave simulations of the unit cell.

The refractive index is plotted in Figure 3 (a), which shows a value of about −1.36 since the imaginary part is very close to zero. Figure 3 (b) shows the complex permittivity and permeability values of the simulated unit cell. The Jerusalem cross metamaterial cell presents a left-handed behavior since the permittivity and permeability are negative.

Figure 4 shows the electric and magnetic fields plotted in the SiO_2 insulation layer for the two different simulations carried out. Figures 4a and 4b correspond to the E and H fields, respectively, when only one isolated Jerusalem cross unit cell was simulated, and Figures 4c and 4d show these fields when the array of Jerusalem cross unit cells (or metasurface) are placed above the monopole antenna.

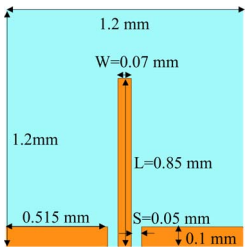

Figure 1. Monopole antenna without metasurface.

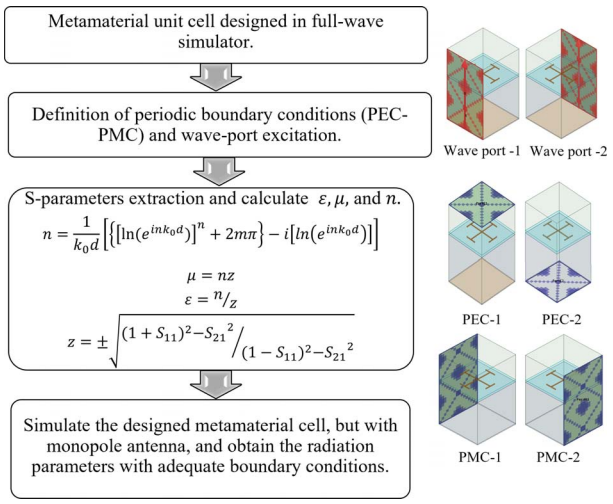

Figure 2. Methodology for unit cell design and simulation.

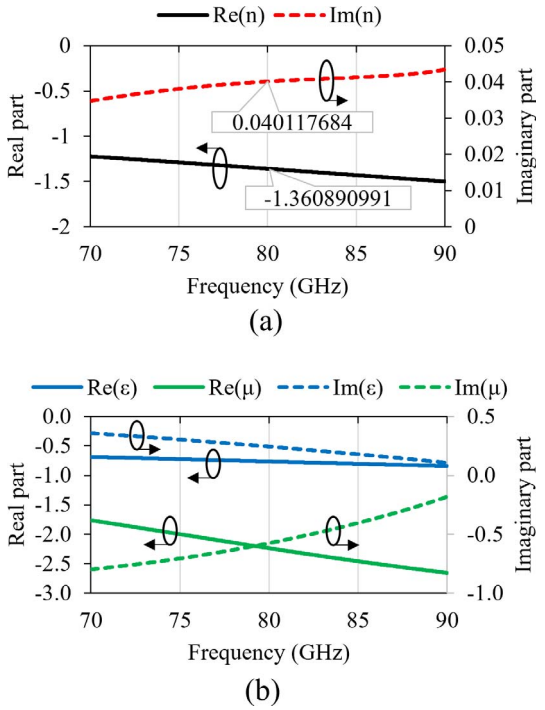

Figure 3. (a) Complex refractive index and (b) complex permittivity (ε) and permeability (μ) versus frequency from simulated metamaterial unit cell (Jerusalem cross).

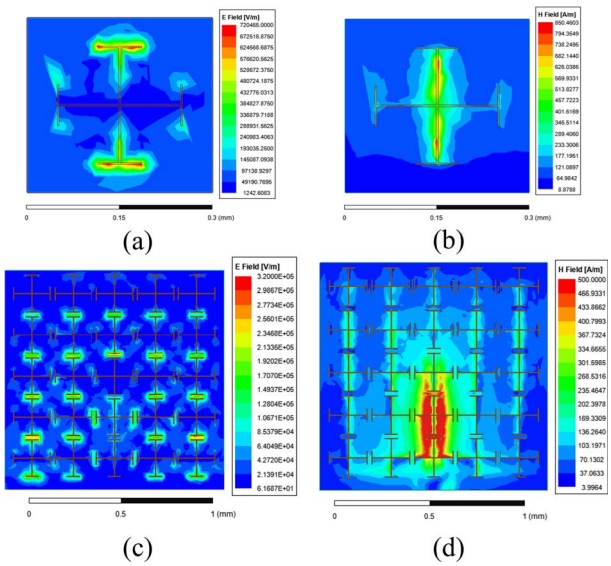

Figure 4. Electric and magnetic fields. (a) E-field; (b) H-field, simulation of metamaterial unit cell using PEC-PMC boundary conditions; (c) E-field; and (d) H-field, simulation of monopole antenna and metamaterial array above using radiation boundary condition.

Comparing the field distribution of (a) versus (c) and (b) versus (d) from Figure 4, it is easy to see the similarity even though the boundary conditions, the geometry, and the excitation are different. Thus, we can assert that the simulation of the unit cell was performed correctly.

These figures show that the electric field is concentrated between each metamaterial cell and that the magnetic field is concentrated along them. The metasurface "catches" the electromagnetic field, being then concentrated above the monopole, that is, in the substrate with the lowest loss (SiO_2) instead of in the substrate with the higher loss (HR-Si).

Figure 5a depicts the top view of the proposed enhanced monopole antenna and its appropriate dimensions. Moreover, Figure 5b shows the top view of the metamaterial unit cell and Figure 5c the cross-sectional view of this design, which was built on a high-resistivity silicon wafer and silicon dioxide with two/three copper metal layers.

Most of the known material properties were incorporated during the design process, such as finite metal conductivity ($\sigma_{Cu} = 5.8 \times 10^7 s/\mathrm{m}$), dielectric loss coefficient ($\tan\delta_{\mathrm{SiO_2}} = 0.001$, $\tan\delta_{\mathrm{HR-Si}} = 0.01$), dielectric constant ($\varepsilon_{r\mathrm{HR-Si}} = 11.9$, $\varepsilon_{r\mathrm{SiO_2}} = 3.9$), and substrate resistivity ($\rho_{\mathrm{HR-Si}} = 7,000\Omega \cdot \mathrm{cm}$) [23].

3. Results

The reflection coefficient at the input port of the initial design of the monopole antenna topology is plotted in Figure 6. The reflection coefficient of the proposed enhanced monopole antenna is also superimposed on the same figure for comparison.

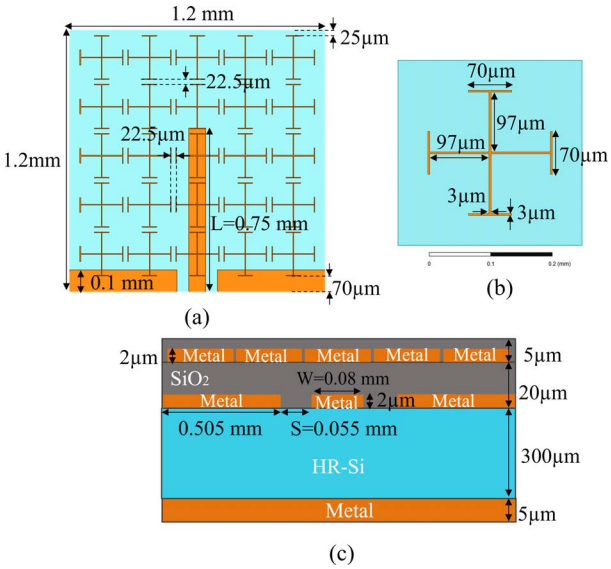

Figure 5. (a) Enhanced monopole antenna for on-chip applications, (b) Jerusalem cross unit cell, and (c) cross-sectional view.

The change in the central frequency of operation is caused by the variation of the effective permittivity and permittivity of the medium; that is, the metamaterials change said parameters, and therefore the frequency shifts. Figure 6 shows the changes in frequency when the metasurface is employed.

Figures 7a–c show the comparison of three principal radiation parameters: gain, directivity, and radiation efficiency versus frequency, respectively, of the monopole antenna with and without metamaterials.

The enhancement of the gain and radiation efficiency are remarkable since the arrangement of Jerusalem cross unit cells causes a change in the electromagnetic field distribution, with the electromagnetic field being concentrated above the monopole, a material with a lower loss.

Moreover, the change in the effective permittivity and effective permeability of the material generates an improvement of the coupling coefficient, which gives rise to a wider impedance bandwidth. Furthermore, since the metallic Jerusalem cross structures reduce the quality factor, the bandwidth increases.

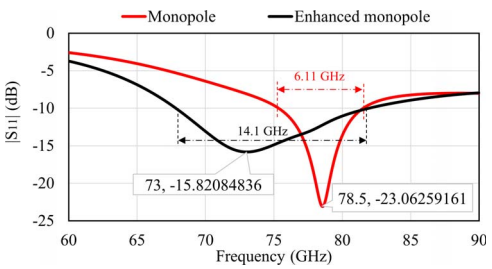

Figure 6. Comparison of reflection coefficient of monopole antenna with and without metamaterials from full-wave simulations.

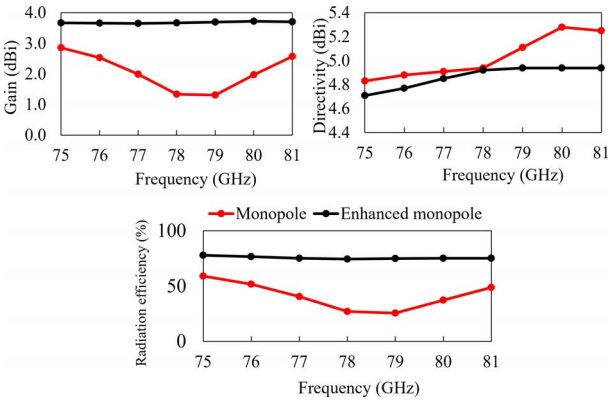

Figure 7. Comparison of gain, directivity, and radiation efficiency between proposed antenna of this work and monopole antenna, from simulation.

Figure 8 shows the two-dimensional radiation patterns generated by the full-wave simulator. The improvement in the radiation pattern shape can be easily noted by the increment in the magnitude of the main lobe and in the enhancement of its symmetry.

Table 1 shows a comparison of the proposed design in this article with other published works. The enhancements achieved in this article are very good since we attain an adequate average gain, good radiation efficiency, and moderate impedance bandwidth while keeping design simple and size compact.

For the implementation of the proposed design, some changes can be done. The ground plane can be replaced with a printed circuit board by placing the chip directly on it; the metal of the monopole and metamaterial cells can be either aluminum or copper in order to be integrated into a HR-SOI-CMOS process, specifically in the uppermost layer of the BEOL. The layer of silicon dioxide can be replaced with another material, such as polyamide or polyimide; however, all dimensions should be adjusted to ensure good performance.

4. Conclusion

The proposed metamaterial-based antenna design in this work shows an easy way to improve the figures of merit of a conventional monopole antenna by

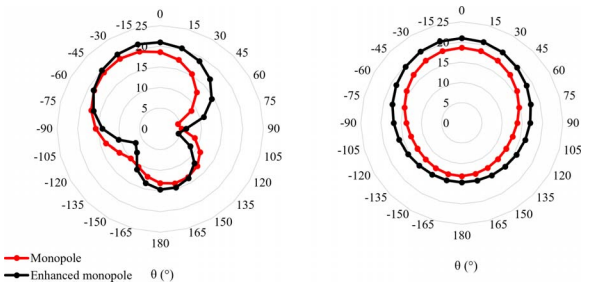

Figure 8. Comparison of two-dimensional radiation patterns (top $\phi = 0^{\circ}$; below $\phi = 90^{\circ}$) at 80 GHz from simulation.

Table 1. Comparison with related works[a]

Parameter	Work					
	[24]	[25]	[26]	[27]	[28]	This work
Operation frequency	77–87 GHz	77 GHz	225 GHz	79–105 GHz	8.3–36.7 GHz	67.83–81.93 GHz
Bandwidth (GHz)	10	6	≥20	26	28.4	14.1
Zin	>120Ω	50Ω	50Ω	N.A.	50Ω	48.2Ω
Gain (dBi)	1.61	11.5	−18	2.29	−3	3.68_{avg}
Radiation efficiency (%)	N.A.	N.A.	1.2	N.A.	N.A.	75.6_{avg}
Total area	16 cm^2	400 mm^2	100 mm^2	1.42 mm^2	15.2 mm^2	1.4 mm^2
Substrate	SiGe RO4003	Duroid 5880 SOI	Si SiO_2	Si SiO_2	Si SiO_2 Si_3N_4	Si-HR SiO_2

[a] N.A. = not available; avg = average value.

exploiting metamaterial properties without an increase in the size or in manufacturing complexity. The proposed enhanced monopole operates from 67.83 GHz to 81.93 GHz over a high-resistivity silicon wafer and a silicon dioxide insulating layer, entirely adequate for on-chip E- and W-band applications. The proposed structure has an acceptable value of bandwidth and gain, with a considerably good radiation efficiency. The design offers a low-cost alternative for on-chip integrated antennas to be used for a host of applications in this frequency range. The design is suitable for its implementation on the HR-SOI-CMOS process with slight modifications.

5. Acknowledgment

The authors thank the Mexican National Council for Science and Technology (CONACyT) for its financial support of this project under grants 852217 and 285199.

6. References

1. P. Kumar, T. Ali, and M. M. M. Pai, "Electromagnetic Metamaterials: A New Paradigm of Antenna Design," *IEEE Access*, **9**, 2021, pp. 18722-18751, doi: 10.1109/ACCESS.2021.3053100.
2. S. Panigrahi and H.-T. Chou, "Leaky Surface Waves Suppression Using Simple Planar Patch-Type AMC Surfaces," 2022 IEEE International Symposium on Antennas and Propagation and USNC-URSI Radio Science Meeting (AP-S/URSI), Denver, CO, USA, 10–15 July 2022, pp. 1388-1389, doi: 10.1109/AP-S/USNC-URSI47032.2022.9886269.
3. M. Dwivedi and D. K. Vishwakarma, "Comparative Study of Conformal Hybrid HIS Based Antennas Performance in 5G Band," 2022 IEEE International Symposium on Antennas and Propagation and USNC-URSI Radio Science Meeting (AP-S/URSI), Denver, CO, USA, 10–15 July 2022, pp. 1870-1871, doi: 10.1109/AP-S/USNC-URSI47032.2022.9886473.
4. M. Tanabe, "Spiral Antenna With a Circular HIS Reflector Sandwiched by Ring-Shaped Absorbers," 2022 IEEE-APS Topical Conference on Antennas and Propagation in Wireless Communications (APWC), Cape Town, South Africa, 05–09 September 2022, pp. 027-029, doi: 10.1109/APWC49427.2022.9899965.
5. P. Wang, J. Liu, G. Huang, Q. Wu, C. Zhou, and W. Wang, "Wideband Gain Enhancement of High-Isolation and Quasi-Omnidirectional Metamaterial MIMO Antenna for Vehicular Radar," *IEEE Transactions on Instrumentation and Measurement*, 2022, doi: 10.1109/TIM.2022.3210989.
6. S. Soily, M. J. Alam, and S. I. Latif, "A High Gain Circularly Polarized Pin Loaded Microstrip Patch Antenna With DNG Metamaterial as Superstrate," 2022 IEEE International Symposium on Antennas and Propagation and USNC-URSI Radio Science Meeting (AP-S/URSI), Denver, CO, USA, 10–15 July 2022, pp. 1454-1455, doi: 10.1109/AP-S/USNC-URSI47032.2022.9887268.
7. H. Wasel and Z. Guoping, "Enhancing 5G Patch Array Antenna Gain Using DNG Metamaterial," *International Journal of Energy Engineering*, **8**, 4, 2018, pp. 93-96.
8. Z. Liu, H. Liu, and Y. Luo, "An Active Metamaterial Antenna With Tunable Zero-Order Resonances," 2022 Photonics and Electromagnetics Research Symposium (PIERS), Hangzhou, China, 25–29 April 2022, pp. 935-940, doi: 10.1109/PIERS55526.2022.9793108.
9. L. B. Pratap, A. Mohan, and A. De, "Compact Bandwidth-Extended CRLH-TL Based Monopole Antenna," 2022 IEEE International Symposium on Antennas and Propagation and USNC-URSI Radio Science Meeting (AP-S/URSI), Denver, CO, USA, 10–15 July 2022, pp. 1062-1063, doi: 10.1109/AP-S/USNC-URSI47032.2022.9886783.
10. K. Iqbal and Q. U. Khan, "Review of Metasurfaces Through Unit Cell Design and Numerical Extraction of Parameters Along With Their Applications in Antenna's Parameters Improvement," *IEEE Access*, **10**, 2022, doi: 10.1109/ACCESS.2022.3214319.
11. Y. G. Adhiyoga, S. F. Rahman, C. Apriono, and E. T. Rahardjo, "Miniaturized 5G Antenna With Enhanced Gain by Using Stacked Structure of Split-Ring Resonator Array and Magneto-Dielectric Composite Material," *IEEE Access*, **10**, 2022, pp. 35876-35887, doi: 10.1109/ACCESS.2022.3163285.
12. M. Aboualalaa, I. Mansour, and R. K. Pokharel, "Dual-Band Split-Ring Antenna With High-Gain Endfire Radiation Characteristics for 5G mm-Wave Applications," 2022 IEEE International Symposium on Antennas and Propagation and USNC-URSI Radio Science Meeting (AP-S/URSI), Denver, CO, USA, 10–15 July 2022, pp. 1050-1051, doi: 10.1109/AP-S/USNC-URSI47032.2022.9887224.
13. C. Milias et al., "Miniaturized Multiband Metamaterial Antennas With Dual-Band Isolation Enhancement," *IEEE Access*, **10**, 2022, pp. 64952-64964, doi: 10.1109/ACCESS.2022.3183800.
14. J. Hasch, U. Wostradowski, S. Gaier, and T. Hansen, "77 GHz Radar Transceiver With Dual Integrated Antenna

Elements," German Microwave Conference Digest of Papers, Berlin, March 2010.
15. A. C. Bunea, D. Neculoiu, A. Stavrinidis, G. Stavrinidis, A. Kostopoulos, and G. Konstantinidis, "Monolithic Integrated Schottky Diode Multiplier and Rectenna for Wireless Communication Link in the W Band," *IEEE Access*, **10**, 2022, pp. 107386-107394, doi: 10.1109/ACCESS.2022.3212772.
16. S. Mukherjee, Z. Su, L. Udpa, S. Udpa, and A. Tamburrino, "Enhancement of Microwave Imaging Using a Metamaterial Lens," *IEEE Sensors Journal*, **19**, 13, 2019, pp. 4962-4971, doi: 10.1109/JSEN.2019.2903454.
17. T. Meyer, W. Hartner, and M. Wojnowski, "On-Chip Antennas for Semiconductor Devices and Related Manufacturing Methods," US Patent 2019/0221531, July 18, 2019.
18. L. Dussopt, "Integrated Antennas and Antenna Arrays for Millimetre-Wave High Data-Rate Communications," 2011 Loughborough Antennas and Propagation Conference, Loughborough, UK, November 14–15, 2011, pp. 1-5.
19. H. Jalli Ng, R. Wang, and K. Kissinger, "On-Chip Antennas in SiGe BiCMOS Technology: Challenges, State of the Art and Future Directions," Asia-Pacific Microwave Conference, Kyoto, Japan, November 06–09, 2018, pp. 621-623.
20. M. K. Hedayati, A. Abdipour, R. S. Shirazi, M. J. Ammann, M. John, C. Cetintepe, and R. B. Staszewski, "Challenges in On-Chip Antenna Design and Integration With RF Receiver Front-End Circuitry in Nanoscale CMOS for 5G Communication Systems," *IEEE Access*, **7**, 2019, pp. 43190-43204.
21. S. Kamaljeet, "Study the Loss of Microstrip on Silicon," *Microwaves & RF*, **56**, April 2017, p. 68.
22. A. B. Numan and M. S. Sharawi, "Extraction of Material Parameters for Metamaterials Using a Full-Wave Simulator," *IEEE Antennas and Propagation Magazine*, **55**, 5, October 2013, pp. 202-211.
23. Y. R. Yuan, H. C. Yuan, S. Y. Kuin, W. M. Hang, and W. H. Wei, "Loss Characteristics of Silicon Substrate With Different Resistivities," *Microwave and Optical Technology Letters*, **48**, 9, June 2006, pp. 1773-1776.
24. C. Mustacchio, L. Boccia, E. Arnieri, and G. Amendola, "Gain Enhancement Technique for On-Chip Monopole Antenna," 50th European Microwave Conference (EuMC), Utrecht, Netherlands, 12–14 January 2021, pp. 650-653.
25. O.-Y. Kwon, C. Cui, J.-S. Kim, J.-H. Park, R. Song, and B.-S. Kim, "A Compact Integration of a 77 GHz FMCW Radar System Using CMOS Transmitter and Receiver Adopting On-Chip Monopole Feeder," *IEEE Access*, **7**, 2019, pp. 6746-6757, doi: 10.1109/ACCESS.2018.2890268.
26. R. S. Narde, J. Venkataraman, and A. Ganguly, "Disc-Loaded, Vertical Top-Hat Monopole Antenna at 225 GHz for On-Chip Wireless Communications," 2019 IEEE International Symposium on Antennas and Propagation and USNC-URSI Radio Science Meeting, Atlanta, GA, USA, 07–12 July 2019, pp. 1883-1884, doi: 10.1109/APUSNCURSINRSM.2019.8889270.
27. C. Mustacchio, L. Boccia, E. Arnieri, and G. Amendola, "W-Band On-Chip Monopole Antenna in Standard 0.13 μm SiGe BiCMOS Technology," 2019 14th International Conference on Advanced Technologies, Systems and Services in Telecommunications (TELSIKS), Nis, Serbia, 23–25 October 2019, pp. 138-140, doi: 10.1109/TELSIKS46999.2019.9002348.
28. S. Mandal, H. Singh, S. K. Mandal, R. Mahapatra, and A. K. Mal, "Design of a Compact Monopole On-Chip Antenna for 24 GHz Automotive Radar Application," 2019 International Workshop on Antenna Technology (iWAT), Miami, FL, USA, 03–06 March 2019, pp. 115-117, doi: 10.1109/IWAT.2019.8730630.